Bull. Mater. Sci., Vol. 36, No. 1, February 2013, pp. 99–105. © Indian Academy of Sciences.

Laser cladding of Zr-based coating on AZ91D magnesium alloy for improvement of wear and corrosion resistance

KAIJIN HUANG[1,2,3,4,*], XIN LIN[2], CHANGSHENG XIE[1] and T M YUE[4]

[1]State Key Laboratory of Materials Processing and Die & Mould Technology, Huazhong University of Science and Technology, Wuhan 430074, P. R. China

[2]State Key Laboratory of Solidification Processing, Northwestern Polytechnic University, Xi'an 710072, P. R. China

[3]Hubei Key Laboratory of Hydroelectric Machinery Design & Maintenance, China Three Gorges University, Yichang 443002, P. R. China

[4]Department of Industrial and Systems Engineering, Hong Kong Polytechnic University, Hung Hom, Hong Kong

MS received 15 March 2011; revised 8 May 2012

Abstract. **To improve the wear and corrosion resistance of AZ91D magnesium alloy, Zr-based coating made of Zr powder was fabricated on AZ91D magnesium alloy by laser cladding. The microstructure of the coating was characterized by XRD, SEM and TEM techniques. The wear resistance of the coating was evaluated under dry sliding wear test condition at room temperature. The corrosion resistance of the coating was tested in simulated body fluid. The results show that the coating mainly consists of Zr, zirconium oxides and Zr aluminides. The coating exhibits excellent wear resistance due to the high microhardness of the coating. The main wear mechanism of the coating and the AZ91D sample are different, the former is abrasive wear and the latter is adhesive wear. The coating compared to AZ91D magnesium alloy exhibits good corrosion resistance because of the good corrosion resistance of Zr, zirconium oxides and Zr aluminides in the coating.**

Keywords. **Laser cladding; AZ91D magnesium alloy; Zr-based coating; wear; corrosion; simulated body fluid.**

1. Introduction

It is well known that metals, ceramics, polymers and their composites can serve as biomaterials. All of them have advantages and disadvantages, for example, metals used as implants have high impact strength, high resistance to wear, ductile and low biocompatibility, corrosion in physiological environment, mismatch for mechanical properties with soft connective tissue; ceramics used as implants have good biocompatibility, inert, corrosion resistance, high tensile strength and undesirable surface properties, special techniques are needed for material fabrication; polymers used as implants have low density, easy to fabricate and low mechanical strength, additives, oligomers may cause tissue reactions (Balamurugan *et al* 2008). Among these, metals such as stainless steels, titanium alloys and cobalt-based alloys are suitable for load-bearing applications compared with ceramics or polymers due to their combination of high mechanical strength and excellent fracture toughness. However, the conventional metallic biomaterials have a risk of releasing toxic metallic ions and/or particles through corrosion or wear process that lead to inflammatory cascades which reduce biocompatibility and cause tissue loss, and the elastic moduli of the conventional metallic biomaterials are not well matched with that of natural bone tissue, resulting in stress shielding effect that can lead to reduced stimulation of new bone growth and remodelling which decreases implant stability (Staiger *et al* 2006; Zeng *et al* 2008).

To improve the wear and corrosion resistance of conventional metallic biomaterials, many surface treatment processes such as shot-peening, laser shock peening, nitriding, ion implantation, passivation, electropolishing, chemical oxidation, surface nanocrystallization, protective coatings on metallic implants have been adopted (Balamurugan *et al* 2008; Antunes and de Oliveira 2012). However, perhaps the most versatile surface modification method is based on the deposition of protective coatings on metallic implants, and involves the improvement of a variety of material properties, such as biocompatibility, corrosion and wear resistance. For example, the effect of titanium nitride (TiN) and diamond-like carbon (DLC) coatings on the wear and corrosion properties of AISI 316L surgical stainless steel specimens were investigated by Wang *et al* (2010). The TiN layer was deposited using electron-beam plasma-assisted physical vapour deposition while the DLC film was produced by a plasma-assisted chemical vapour deposition method. Both coatings significantly improved the corrosion resistance and wear resistance of the substrate. Nevertheless, it is important to bear in mind that such layers have intrinsic limitations regarding their application as protective films on load-bearing implants. These include the formation of wear debris and the intrinsic brittleness of PVD thin films.

In addition, the bioceramics coating fabricated by different methods such as plasma spray technique, ion beam

*Author for correspondence (huangkaijin@yahoo.com.cn)

assisted deposition, magnetron sputtering, sol–gel and pulsed laser deposition, such as HAP [$Ca_{10}(PO_4)_6(OH)_2$], TCP[$Ca_3(PO_4)_2$] and their bi-phase combinations can reduce the release of toxic or harmful ions from the metal alloys, because the bioceramics coating represents a truly effective barrier that hinders the metallic ion kinetics of release towards the living body (Balamurugan *et al* 2008). However, the poor mechanical properties of calcium phosphates limit the use of the bulk material to non-load bearing implants and are always used to coat inert or biotolerable implants with mechanical properties adequate for orthopaedic substitutions.

Searching among the existing commercially available metals and alloys, we can find that Mg is probably the most appropriate metal that can best fulfil the density and stiffness requirements. Although the attempt failed as the metal corroded too rapidly *in vivo*, interest in using Mg for orthopedic implants has not faded but still remains strong, especially for degradable biomaterials. The reason is that the corrosion rate of Mg and its alloys can be modulated through the use of high purity Mg or new alloying systems (Gao *et al* 2008; Li *et al* 2008; Erinc *et al* 2009; Gu *et al* 2009; Rettig and Virtanen 2009) and surface modification including protective coatings (Song 2007; Chen J *et al* 2008; Majumdar *et al* 2008; Song *et al* 2008; Xin *et al* 2008; Shi *et al* 2009) and surface treatments (Liu *et al* 2007a, b; Hanzi *et al* 2009; Xu *et al* 2009; Wen *et al* 2009). It is considered that if the corrosion problem of Mg can be resolved, Mg or its alloys could become good materials for implantation applications.

In the present study, an attempt has been made to fabricate Zr-based coating made of Zr powder on AZ91D magnesium alloy by laser cladding. Zr was used because Zr and its oxides show excellent electrochemical properties (Gao *et al* 2008; Tsutsumi *et al* 2009), no toxicity (Akahori *et al* 2008; Chen X B *et al* 2008; Gu *et al* 2009) and good biocompatibility (Uchida *et al* 2002a, b; Shi and Hulbert 2002; Liu *et al* 2006; Chen X B *et al* 2008; Han *et al* 2009). It should be pointed out that although PVD, thermal spraying and plasma spraying, etc can also be used to fabricate wear and corrosion resistant coatings on Mg, they have their disadvantages. For example, many pores and weak bonding are the main drawbacks of the coatings fabricated by thermal spraying and plasma spraying. While PVD is a line of sight technique so there are limitations on workpiece geometry, also the coating does not form a metallurgical bond with the substrate. The advantages of laser cladding can fabricate porosity free coatings with a strong metallurgically bonded coating interface. Moreover, multiple powder compositions can be fed simultaneously or sequentially to form the desired properties at specific locations.

2. Experimental

Laser cladding of Zr powder was conducted on AZ91D magnesium alloy. The size of specimen was $50 \times 25 \times 10$ mm. The size of the powder was < 75 μm and the purity of the powder was 99 mass%. The powder was delivered into the laser molten pool with a lateral powder feeder driven by a flow of Ar gas. Laser cladding was performed using a high power PRC CO_2 continuous wave laser. The laser spot diameter, laser power, powder feeding rate and laser scanning velocity were kept constant at 3 mm, 1000 W, 0·08 g/s and 15 mm/s, respectively. A track overlap condition of 30% was used.

The different phases of the Zr-based coating were determined with the X-ray diffraction (XRD) technique using CuKα radiation at 40 kV and 30 mA (X' Pert PRO) and transmission electron microscopy (TEM, FEI Tecnai G220). The microstructure of the coating etched with an aqua regia, the surface morphologies of the worn and corrosive specimens were examined by a Quanta 200 scanning electron microscope (SEM) with energy dispersive X-ray spectroscopy (EDS). Cross-section specimens were prepared for TEM study. A microhardness tester (MICROMET 3) using a test load of 100 g and a load-well time of 15 s was employed to measure the microhardness of the coating.

Although there are some differences between the wet sliding wear under body fluid environment at human body temperature and the dry sliding wear under air environment at room temperature, the wear rate of dry sliding wear is the biggest among all different wear types under the same conditions, so the dry sliding wear resistance of the Zr-based coating was evaluated using a block-on-ring wear tester at room temperature. The cladded specimens for the wear test were cube blocks ($10 \times 10 \times 10$ mm) which were slided against a rotating ring of hardened bearing steel AISI52100 with a hardness of 60 HRC. The test load used was 98 N. The relative sliding speed was at 0·4187 m/s. The wear test cycle lasted for 75 min and the corresponding total wear sliding distance was 1884 m. The as-received AZ91D magnesium alloy was selected as the reference materials for all wear tests. Each test was repeated three times. The wear weight

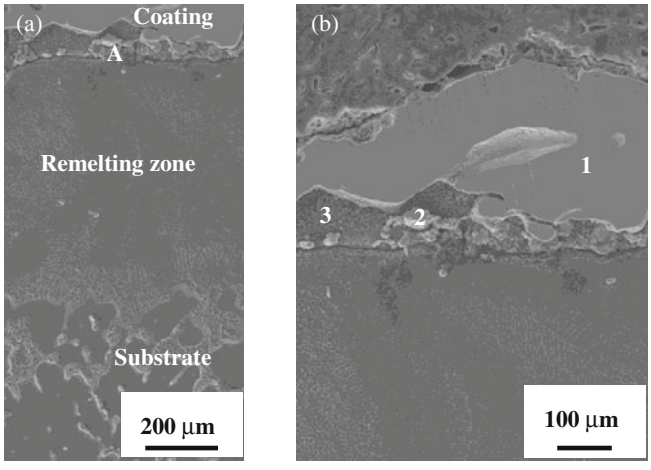

Figure 1. Microstructure of Zr-based coating fabricated by laser cladding: (**a**) cross section of coating and (**b**) higher magnification of region A in **figure 1** (**a**).

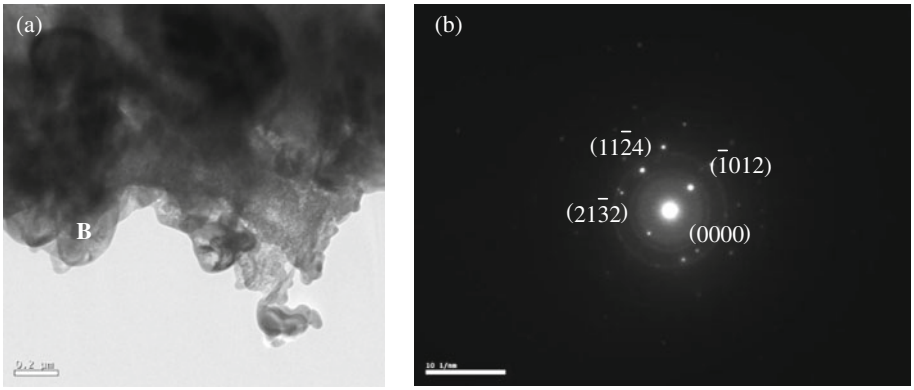

Figure 2. TEM image and SAED patterns of Zr-based coating fabricated by laser cladding: (**a**) Bright field image of coating and (**b**) diffraction pattern from [$\bar{2}6\bar{1}$] of Zr phase at location B in **figure 2** (**a**).

Table 1. Results of EDS analysis of Zr-based coating.

Position	Zr (mass%)	Mg (mass%)	Al (mass%)	O (mass%)
1	72·50	–	23·75	3·75
2	82·82	–	10·25	6·93
3	–	82·00	11·70	6·30
B	96·40	–	3·30	0·30

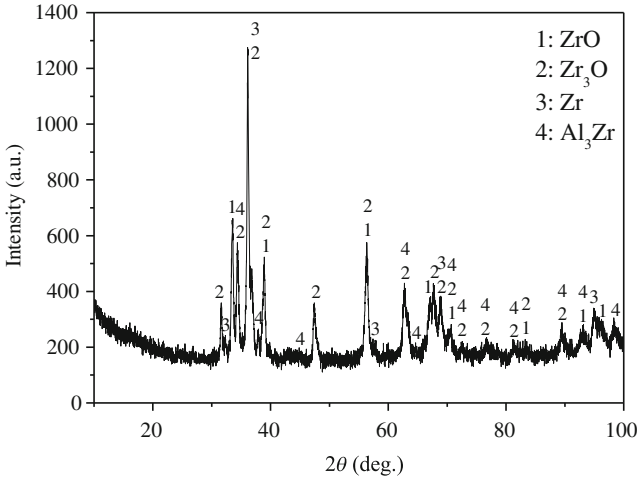

Figure 3. XRD patterns of Zr-based coating fabricated by laser cladding.

loss was measured using an electronic balance (Bartorius BS110) with an accuracy of 0·1 mg.

The potentio-dynamic polarization test was employed to evaluate the corrosion behaviour of the Zr-based coating. The test was conducted in simulated body fluid, viz Ringer's solution (8·5 g/L NaCl, 0·25 g/L KCl, 0·22 g/L $CaCl_2$, 0·15 g/L $NaHCO_3$) at pH = 7·4 using saturated calomel electrode (SCE) as reference electrode and platinum as counter electrode. Polarization was carried out at a scan rate of 1 mV/s. Before the polarization test, the specimens were kept in the Ringer's solution for 600 s at 37 °C.

3. Results and discussion

3.1 *Microstructure*

Figure 1 shows microstructure of the Zr-based coating. This figure shows three distinct zones: viz. the coating, the re-melting zone and the substrate. Figure 2 shows a TEM image of an area in the coating with the SAED pattern of Zr particle. Table 1 summarizes the results of the EDS analysis of the coating. Figure 3 shows XRD patterns of the coating. XRD results together with the EDS results and the TEM study suggest that the microstructure of the coating mainly consists of Zr, Zr oxides and Zr aluminides.

During laser cladding, when the high power CO_2 laser reaches the preplaced Zr powder coating, the Zr powder adsorbs CO_2 laser and is heated up to the melting point of Zr (2125 K) quickly and forms liquid Zr. Then, since oxygen in the surrounding environment has a very high affinity to Zr, partial liquid Zr will react with the dissolved oxygen and forms different Zr oxides according to Zr–O phase diagram because its melting temperature is higher than that of the Zr and Al_3Zr (1853 K) phases. In succession, the unwanted liquid Zr will solidify when the temperature of liquid Zr decreases to 2125 K. After the Zr oxides and Zr phases are formed one after another, the remaining liquid, which is rich in Al coming from the melted AZ91D substrate, will finally solidify and forms Al_3Zr intermetallic compounds according to Al–Zr phase diagram under the help of high convection velocity of the laser melt pool (Picasso and Hoadley 1994).

In addition, according to the results of the EDS analysis of the coating (table 1), no Mg, but Al was detected in the coating. The explanation is that during laser cladding of the Zr-based coating, the temperature of the processing zone exceeded the melting point of Zr (2125 K), which is higher than the boiling point of Mg (1380 K), but lower than that of Al (2740 K). Under such a condition, when Zr was melted,

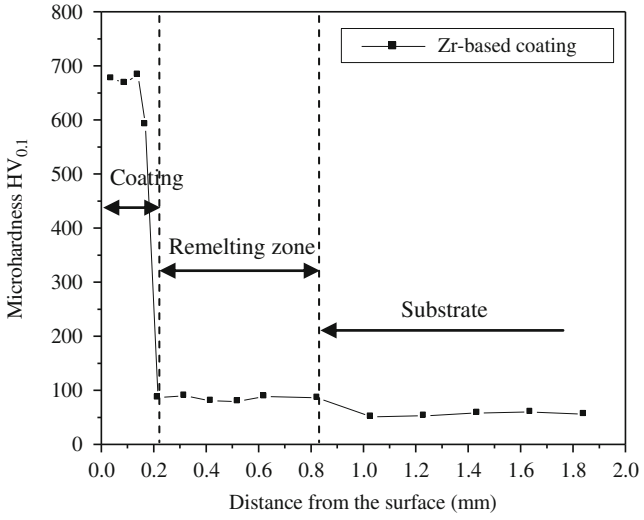

Figure 4. Microhardness of Zr-based coating fabricated by laser cladding.

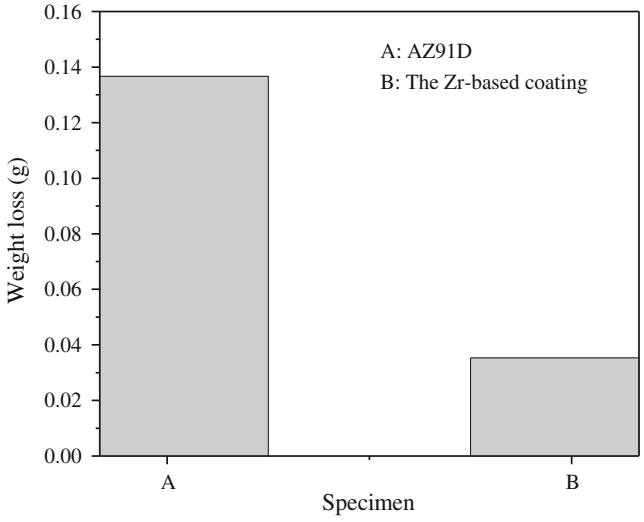

Figure 5. Weight loss of different specimens under dry wear conditions at room temperature.

the surrounding Mg would be vapourized leaving Al in the melt pool to react with Zr. The microhardness of the Zr-based coating was very high (figure 4) because the coating consists of Zr oxides and Al_3Zr phases of high hardness, and is about 6–7 times higher than that of the AZ91D substrate.

3.2 *Wear properties*

Figure 5 shows weight loss of the Zr-based coating specimen and the AZ91D material without a coating, i.e. untreated, under dry wear conditions. The weight loss of the Zr-based coating specimen was lower than that of the untreated AZ91D specimen. In other words, the wear resistance of the Zr-based coating was obviously better than that of AZ91D specimen because the weight loss of AZ91D specimen is about 3·9 times higher than that of the Zr-based coating specimen. The wear resistance results of different specimens are consistent with the corresponding microhardnesses of different specimens (figure 4), and the higher microhardness, the better wear resistance.

The Zr-based coating mainly consists of Zr, Zr oxides and Zr aluminides (figure 3). The microstructure provided the coating with an excellent wear resistance under dry wear condition, as indicated in figures 5 and 6. As shown in figure 6, the worn surface of the untreated AZ91D specimen suffered from severe adhesive wear and the worn surface of the Zr-based coating specimen experienced severe abrasive wear. The former is evident by the feature of heavy plastic deformation (figure 6a) and the large mass wear rate ($3{\cdot}04 \times 10^{-8}$ kg/s). The latter is evident by the relatively mild plastic deformation but with many small particles of wear debris found at the surface (figure 6b) and the small mass wear rate ($7{\cdot}84 \times 10^{-9}$ kg/s). The results of the EDS analysis showed that these particles were mainly composed of iron oxides (table 2). Apparently, the above characteristics of the worn surfaces are related to the surface microhardness of different specimens.

It is indicated that under the condition of room temperature dry sliding wear test, the surface of an untreated

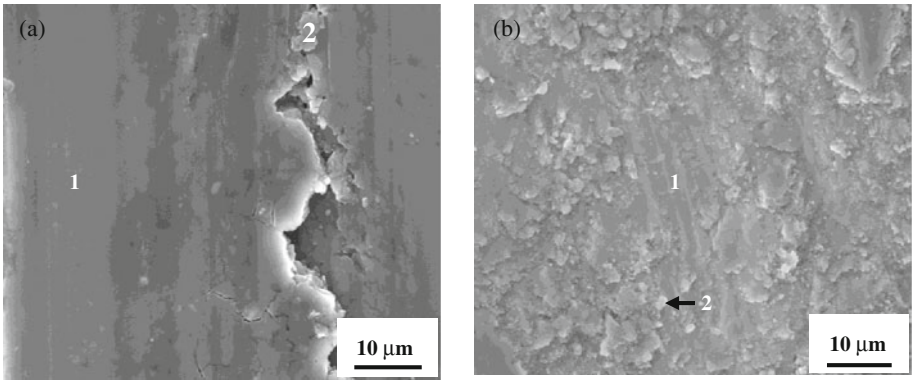

Figure 6. SEM images of worn surfaces of different specimens: (**a**) untreated specimen AZ91D and (**b**) Zr-based coating specimen.

Table 2. EDS results of worn surface (mass%).

Sample	Position	C	O	Mg	Al	Zn	Fe	Zr	Mn
AZ91D	1	2·86	8·64	82·18	5·68	0·64	–	–	–
AZ91D	2	2·08	14·86	77·52	4·36	0·72	0·46	–	–
Zr-based coating	1	1·08	6·42	1·38	6·46	–	13·70	70·96	–
Zr-based coating	2	1·02	38·40	0·30	0·40	–	59·20	0·68	–
AZ91D	Raw	–	–	90·16	8·95	0·63	–	–	0·26

specimen AZ91D would first adhere to the surface of the hardened AISI52100 steel ring and then smeared off because of its low hardness of the untreated specimen AZ91D (figure 4). On the other hand, the worn surface of the Zr-based coating was covered with wear debris particles including iron oxides (figure 6b and table 2). Such results were not observed on the untreated AZ91D sample.

In normal sliding tests, there is a material-to-material contact, followed by welding or fusing of the contacting asperities. When sliding continues, the asperities of the weaker material may shear off and transfer to the opposite surface (Kelly *et al* 1998). In the present work, in case of the untreated specimen AZ91D, the hardened AISI52100 steel ring, whose main constituent is Fe, shears the soft magnesium phase off; as a result, small content of iron is deposited on the worn surface (table 2). On the contrary, the microhardness of the Zr-based coating (figure 4) is almost the same as the hardened AISI52100 steel ring, and the material from the ring is sheared off, as a result, large content of iron is deposited on the worn surface (table 2). At the same time, the Zr, Zr oxides and Zr aluminides would be broken up by the dry sliding action and smeared along the surface.

In conclusion, according to the morphologies of the worn surfaces (figure 6) and the results of EDS (table 2), the dominant type of wear mechanism of the relatively soft untreated AZ91D is considered to be adhesive wear process. On the other hand, the type of wear mechanism of the Zr-based coating specimen is dominated by abrasive wear process. Nevertheless, oxidation and friction wear might also be involved in cases of the untreated specimen AZ91D and the Zr-based coating specimen.

3.3 *Corrosion properties*

Figure 7 shows potentio-dynamic polarization curves of different specimens. Table 3 lists the corrosion parameters of different specimens in Ringer's solution. The results show that the Zr-based coating is superior to the untreated AZ91D substrate in corrosion properties. For example, the corresponding corrosion potential (E_{corr}) of the Zr-based coating specimen is −0·4425 V, which is 928·1 mV more positive than the corrosion potential of the untreated AZ91D substrate. The open-circuit corrosion current density (I_{corr}) of the untreated AZ91D substrate is about 923·4 times higher than that of the Zr-based coating. The corresponding polarized resistance (R_p) of the Zr-based coating is about 351·7

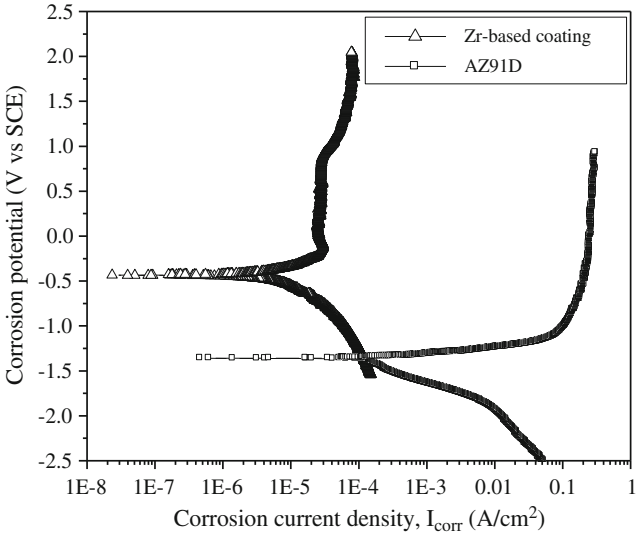

Figure 7. Potentiodynamic polarization curves of different specimens in Ringer's solution.

times higher than that of the untreated AZ91D substrate. The corrosion rate (CR) of the untreated AZ91D substrate is about 228·1 times higher than that of the Zr-based coating. Figure 8 shows SEM morphologies of corrosive surfaces of different specimens.

For AZ91D magnesium alloy, the mass fraction of Mg is about 90 mass% (table 2). Mg is a very active metal, the equilibrium potential of Mg is −2·37 V and the equilibrium potential in conventional media is also very low. Moreover, the oxide film of magnesium is generally loose and porous; therefore, AZ91D magnesium alloy normally has fairly poor corrosion resistance. The electrochemical corrosion of AZ91D magnesium alloy is mainly the process of releasing hydrogen with its quick dissolution.

According to a modified pH-potential diagram of Mg and its alloys in various simulated body fluids, the corrosion attack of magnesium in an aqueous environment can be expressed as the following partial reactions (Zeng *et al* 2008):

$$\text{Anodic reaction: } Mg \rightarrow Mg^{2+} + 2e,$$

$$\text{Cathodic reaction: } 2H_2O + 2e \rightarrow 2OH^- + H_2,$$

$$\text{Production formation: } Mg^{2+} + 2OH^- \rightarrow Mg(OH)_2,$$

$$\text{General reaction: } Mg + 2H_2O \rightarrow Mg(OH)_2 + H_2.$$

Table 3. Corrosion parameters of different specimens in Ringer's solution.

Specimen	E_{corr} (V)	I_{corr} (A/cm^2)	R_p (Ω/cm^2)	CR (mm/year)
AZ91D	−1·3706	0·0008971	29·079	14·697
Zr-based coating	−0·4425	0·000009175	10228	0·06442

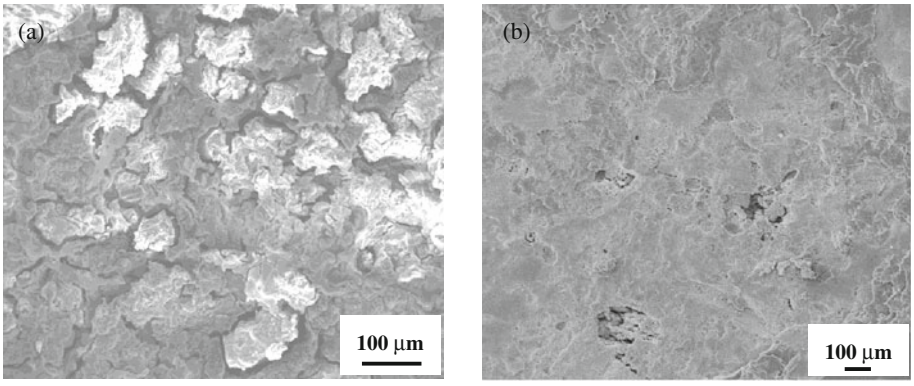

Figure 8. SEM images of corroded surfaces of different specimens: (**a**) untreated specimen AZ91D and (**b**) Zr-based coating specimen.

Therefore, the dissolution of Mg in simulated body fluid goes with the release of H_2. This can be proved by the phenomena that many gas bubbles produced when the untreated specimen AZ91D was put in the simulated body fluid. It should be pointed out that the amount of gas bubbles decreased with the increase of time, and this explained the decrease of the dissolution of Mg in simulated body fluid because the production of OH^- ion resulted in the increase of pH of simulated body fluid from pH = 7·4 to pH = 10·5 in the end. On the other hand, Cl^- ions in simulated body fluid can destroy the gray-oxide film of $Mg(OH)_2$ and reacts with Mg. The following reactions summarize the corrosion reactions of Mg (Staiger *et al* 2006):

$$Mg(s) + 2H_2O \rightarrow Mg(OH)_2(s) + H_2(g),$$

$$Mg(OH)_2(s) + 2Cl^- \rightarrow MgCl_2 + 2OH^-,$$

$$Mg(s) + Cl^-(aq.) \rightarrow MgCl_2.$$

So, the corrosion of AZ91D magnesium alloy is severe (table 3 and figure 8(a)).

The relatively better corrosion property of the Zr-based coating compared with the untreated AZ91D substrate is related to the presence of excellent corrosion resistance of Zr (Subramanian *et al* 1991; Gao *et al* 2008; Tsutsumi *et al* 2009), Zr oxides (Balamurugan *et al* 2003; Namgung *et al* 2010) and Zr aluminides (Nguyen-Manh and Pettifor 1999). This can be proved by the phenomena that there was no obvious microstructure morphology in the coating etched with an aqua regia (figure 1). Of course, microgalvanic corrosion also exists in the Zr-based coating due to different crystalline phases and a small quantity of corrosion products are kept on the corrosive surface (figure 8(b)).

4. Conclusions

Based on Zr powder, a high wear and corrosion resistant Zr-based coating has been successfully fabricated by laser cladding on AZ91D magnesium alloy. The Zr-based coating is mainly composed of Zr, Zr oxides and Al_3Zr phases. Under the dry sliding wear condition at room temperature, the wear resistance of the Zr-based coating was considerably higher than that of the untreated AZ91D material, and the weight loss of the AZ91D substrate was about 3·9 times higher than that of the Zr-based coating. The main wear mechanisms of the coating and the AZ91D sample are different, the former was abrasive wear and the latter was adhesive wear. The Zr-based coating has superior corrosion resistance when compared to the untreated AZ91D material in the simulated body fluid. The corrosion rate (CR) of the untreated AZ91D material was about 228·1 times higher than that of the Zr-based coating.

Acknowledgements

This work was supported by the Fund (SKLSP201108) of the State Key Laboratory of Solidification Processing in NWPU, the Fund (2010-P07) of the State Key Laboratory of Materials Processing and Die & Mould Technology in HUST,

the Foundation (2008007) of Key Laboratory for Advanced Materials Processing Technology in Tsinghua University, and the Fund (2010KJX01) of the Hubei Key Laboratory of Hydroelectric Machinery Design & Maintenance in China Three Gorges University. The authors are also grateful to Analytical and Testing Centre of Huazhong University of Science and Technology.

References

Akahori T, Niinomi M, Nakai M, Kasuga T and Ogawa M 2008 *Mater. Trans.* **49** 365

Antunes R A and de Oliveira M C L 2012 *Acta Biomater.* **8** 937

Balamurugan A, Kannan S and Rajeswari S 2003 *Mater. Lett.* **57** 4202

Balamurugan A, Rajeswari S, Balossier G, Rebelo A H S and Ferreira J M F 2008 *Mater. Corros.* **59** 855

Chen J, Zeng R C, Huang W J, Zheng Z Q, Wang Z L and Wang J 2008 *Trans. Nonferrous Met. Soc. China* **18** S361

Chen X B, Nouri A, Li Y C, Lin J G, Hodgson P D and Wen C 2008 *Biotechnol. Bioeng.* **101** 378

Erinc M, Sillekens W H, Mannens R G T M and Werkhoven R J 2009 *Applicability of existing magnesium alloys as biomedical implant materials*. in *Proceeding* (eds) E A Nyberg *et al* (New York: TMS) p. 209

Gao J C, Wu S, Qiao L Y and Wang Y 2008 *Trans. Nonferrous Met. Soc. China* **18** 588

Gu X N, Zheng Y F, Cheng Y, Zhong S P and Xi T F 2009 *Biomaterials* **30** 484

Han Y, Yan Y Y, Liu G G, Zhang Y M and Xu K M 2009 *J. Biomed. Mater. Res.* **A88** 117

Hanzi A C, Gunde P, Schinhammer M and Uggowitzer P J 2009 *Acta Biomater.* **5** 162

Kelly J, Nagarathnam K and Mazumder J 1998 *J. Laser Appl.* **10** 45

Li Z J, Gu X N, Lou S Q and Zheng Y F 2008 *Biomaterials* **29** 1329

Liu X Y, Huang A P, Ding C X and Chu P K 2006 *Biomaterials* **27** 3904

Liu C L, Xin Y C, Tang G Y and Chu P K 2007a *Mater. Sci. Eng. A* **456** 350

Liu C L, Xin Y C, Tian X B, Zhao J and Chu P K 2007b *J. Vac. Sci. Technol. A* **25** 334

Majumdar J D, Bhattacharyya U, Biswas A and Manna I 2008 *Surf. Coat. Technol.* **202** 3638

Namgung S, Ko Y G, Shin K R and Shin D H 2010 *Korean J. Met. Mater.* **48** 813

Nguyen-Manh D and Pettifor D G 1999 *Intermetallics* **7** 1095

Picasso M and Hoadley A F A 1994 *Int. J. Numer. Meth. Heat Fluid Flow* **4** 61

Rettig R and Virtanen S 2009 *J. Biomed. Mater. Res.* **A88** 359

Shi P, Ng W F, Wong M H and Cheng F T 2009 *J. Alloys Compds.* **469** 286

Shi X F and Hulbert S 2002 *Biomed. Sci. Instrum.* **38** 489

Song G L 2007 *Adv. Mater. Res.* **29** 95

Song Y W, Shan D Y and Han E H 2008 *Mater. Lett.* **62** 3276

Staiger M P, Pietak A M, Huadmai J and Dias G 2006 *Biomaterials* **27** 1728

Subramanian R, Sircar S and Mazumder J 1991 *J. Mater. Sci.* **26** 951

Tsutsumi Y, Nishimura D, Doi H, Nomura N and Hanawa T 2009 *Mater. Sci. Eng. C* **29** 1702

Uchida M, Kim H M, Miyaji F, Kokubo T and Nakamura T 2002a *Biomaterials* **23** 313

Uchida M, Kim H M, Kokubo T, Tanaka K and Nakamura T 2002b *J. Ceram. Soc. Jpn* **110** 710

Wang L, Su J F and Nie X 2010 *Surf. Coat. Technol.* **205** 1599

Wen C L, Guan S K, Peng L, Ren C X, Wang X and Hu Z H 2009 *Appl. Surf. Sci.* **255** 6433

Xin Y C, Liu C L, Zhang W J, Jiang J, Tang G Y, Tian X B and Chu P K 2008 *J. Electrochem. Soc.* **155** C178

Xu L P, Zhang E L and Yang K 2009 *J. Mater. Sci.: Mater. Med.* **20** 859

Zeng R C, Dietzel W, Witte F, Hort N and Blawert C 2008 *Adv. Biomater.* **10** B3